Galvanomagnetic Tensors of Bismuth Single Crystals at Low Temperatures

Galvanomagnetic Tensors of Bismuth Single Crystals at Low Temperatures

Shôichi MASE

Department of General Education, Nagoya University

and Seiichi TANUMA

Research Institute for Iron, Steel and Other Metals, Tôhoku University

(Received November 19, 1959)

Synopsis

A measurement of the galvanomagnetic tensors of bismuth at the liquid helium temperature and in the magnetic field up to 10 kilo Oersted is reported of three single crystals with different crystallographic orientations. All non-vanishing tensor components (except one) predicted by the crystal symmetry and Onsager's reciprocal relation are measured. The dependency of the symmetric tensor components on the direction of the magnetic field is studied somewhat in detail. The experimental results are analysed semi-phenomenologically on the basis of the Boltzmann equation. Our experimental results of the absolute values and the field dependencies for the symmetric and antisymmetric tensor components respectively are such as expected theoretically in chemically pure samples. The anisotropy of the tensor components of typical type is, however, fairly small compared with that expected from the known energy surface anisotropy. This shows the importance of the anisotropic scattering or a failure of usual approximate theory, but unfortunately we could not obtain quantitative conclusion because a part of each anisotropy should have been attributed to undesirable boundary effect and other effects.

I. Introduction

Since several years ago, the oscillatory phenomena of the galvanomagnetic effect in metals at low temperatures have been called to the attention by many researchers in connection with the oscillations of magnetic susceptibility and other effects. Particularly those of bismuth have been extensively studied by several authors.[1)-5)] These studies, however, were mainly confined to the oscillating part and did not give so much attention of the relation between the oscillating part and the non-oscillating part. This may be partly due to the fact that the oscillating part of bismuth could be analysed satisfactorily[6)] (or apparently) by assuming the shape of the energy surface of electrons or holes which are responsible for the oscillation but the non-oscillating part colud not be explained without a detailed knowledge on the entire Fermi surface. It is noted, however, that the

(1) P. B. Alers and R. T. Webber: Phys. Rev. **91** (1953) 1060.
(2) J. M. Reynolds, H. W. Hemstreet, T. E. Leinhardt, and D. D. Triantos: Phys. Rev. **96** (1954) 1203.
(3) R. A. Connell and J. A. Marcus: Phys. Rev. **107** (1957) 940.
(4) J. Babiskin: Phys. Rev. **107** (1957) 981.
(5) T. Okada: private communication through Busseiron Kenkyu **3** (1958) 313.
(6) D. Shoenberg: Proc. Roy. Soc. **A170** (1939) 341.

theories of the oscillating magnetic susceptibility, galvanomagnetic, and other effects in hand may not be based upon the firm foundation,* at least, for semi-metals as bismuth and graphite, and that their applicability is not yet made so clear. Satisfactory theory should explain quantitatively both non-oscillating and oscillating parts. Any one has yet given no satisfactory result in both an experiment and a theory.

In the present paper we report an experimental study for the galvanomagnetic effect of highly refined bismuth single crystals at the liquid helium temperature and in the magnetic field up to about 10 kilo Oersted. The first object of present study was to obtain the anisotropy of the non-oscillating part in order to test the validity of the assumption of the effective mass approximation usually used in magnetic phenomena, but unfortunately we could not obtain a very satisfactory result in view point of a phenomenological theory, i.e. of the crystal symmetry and the reciprocal relation, because of very difficulty of the technique of measurement in bismuth with very long mean free path in low temperatures. In the present paper, however, we could give qualitative explanation for very remarkable features of the galvanomagnetic tensors of bismuth.

II. Symmetry consideration of galvanomagnetic tensors

Bismuth crystal has the crystallographic symmetry D_{3d}^5. The crystal has one trigonal axis and three binary axes in the perpendicular plane to the trigonal axis We choose one of the binary axes and the trigonal axis as x- and z-axis respectively. The orthogonal axis to them is taken to be y-axis. The crystal is invariant by typical twelve symmetry operations of the space group but in the symmetry consideration of the tensors we may consider the following six point group operations[7]: (i) E (the unit element), (ii) C_3^+ and C_3^- ($\pm 120°$ rotation around the trigonal axis), (iii) U (the rotation by π around x-axis), and (iv) UC_3^+ and UC_3^-.

The relation between the electric field and current is given by the formula

$$E_i = \sum_k \rho_{ik}^s(H) J_k + \sum_{k(\neq i)} \rho_{ik}^a(H) J_k , \tag{1}$$

where E_i is the electric field component, J_k the current density component, and $\rho_{ik}^s(H)$ (or $\rho_{ik}^a(H)$) the symmetric (or antisymmetric) part of the resistivity tensor component. Further there are the following reciprocal relations

$$\rho_{ik}^s(H) = \rho_{ki}^s(-H) , \qquad \rho_{ik}^a(H) = \rho_{ki}^a(-H) . \tag{2}$$

By an operation $\mathfrak{R}$, $\rho_{ik}(H)$ is transformed as

$$\rho_{i'k'}(l') = \mathfrak{R}\rho_{ik}(l) = \sum \frac{\partial i'}{\partial m} \frac{\partial k'}{\partial n} \rho_{mn}(l) , \tag{3}$$

* These are based upon the effective mass approximation. Inadequacy of this approximation in magnetic susceptibility of bismuth was discussed by E. N. Adams: Phys. Rev. 89(1953) 633.

(7) T. Okada (Mem. Fac. Sci. Kyusyu Univ. **B1** (1955) 157) and H. J. Juretschke (Acta Cryst. 8 (1955) 716) gave the tables of the non-vanishing tensor components in *very* weak magnetic field.

where l in the parenthesis is the direction of the magnetic field. If l is invariant by the transformation of the coordinate,

$$\rho_{i'k'}(l') = \rho_{ik}(l)$$

and if l is transformed into negative direction in the new system,

$$\rho_{i'k'}(l') = \rho^s_{ik}(l) - \rho^a_{ik}(l) .$$

With the use of the equations (2) and (3), we can determine the symmetry property of the tensors, i.e. we can obtain non-vanishing terms of $\rho_{ik}(l)$. For example, by the operation U, $\rho_{xy}(x)$ should be invariant, whereas the right hand terms of (3) becomes $-\rho_{xy}(x)$. Then $\rho^s_{xy}(x)$ and $\rho^a_{xy}(x)$ should be both zero. We can do similar argument for the other components.

Thus the galvanomagnetic tensors in the magnetic field parallel to binary (x), bisectrix (y) and trigonal (z) axes are given by

$H//x$-axis

$$\rho(x) = \begin{pmatrix} \rho_{xx}(x) & 0 & 0 \\ 0 & \rho_{yy}(x) & \rho^s_{yz}(x) + \rho^a_{yz}(x) \\ 0 & \rho^s_{yz}(x) - \rho^a_{yz}(x) & \rho_{zz}(x) \end{pmatrix}, \tag{4a}$$

$H//y$-axis

$$\rho(y) = \begin{pmatrix} \rho_{xx}(y) & \rho^a_{xy}(y) & -\rho^a_{zx}(y) \\ -\rho^a_{xy}(y) & \rho_{yy}(y) & \rho^s_{yz}(y) \\ \rho^a_{zx}(y) & \rho^s_{yz}(y) & \rho_{zz}(y) \end{pmatrix}, \tag{4b}$$

$H//z$-axis

$$\rho(z) = \begin{pmatrix} \rho_{xx}(z) & \rho^a_{xy}(z) & 0 \\ -\rho^a_{xy}(z) & \rho_{yy}(z) & 0 \\ 0 & 0 & \rho_{zz}(z) \end{pmatrix}. \tag{4c}$$

The vanishing of some tensor components can be used for the check of the accuracy of the setting of the samples and the apparatus. The symmetric and antisymmetric parts of $\rho_{yz}(x)$ can be separated by reversing the magnetic field as usual.

III. Experimental procedure

The measurements are made mainly at 4.2°K. At this temperature the condition $\omega\tau \gg 1$ may be satisfied at usual magnetic field strength with a moderate purity of the samples (ω is the cyclotron frequency and τ the relaxation time of scattering with imperfection). We are, however, particularly interested in the anisotropy of the galvanomagnetic effect of high purity bismuth, i.e. of bismuth with closely equal number of electrons and holes. In order to satisfy this object the impurity concentration should be less than 10^{-5} per atom.

a) Preparation of the samples

The samples used here were prepared from Tadanac bismuth with the purity of nearly six nine. Tadanac bismuth of about 500 gr was refined by the technique of zone melting repeatedly by twenty four times with the zone-width of about

2 cm and with a speed of about 15 cm per hour. With the use of the central one thirds of the refined ingot, a large single crystal was grown by the Bridgman method. We cut out three samples from this single crystal. The crystallographic orientations were determined by the light figure method. The orientations are shown in Fig. 1. The length of each sample is about 1.2 cm, and a and d are respectively 0.20 and 0.26 cm. The crystal axes may be set out as shown in Fig. 1 within the accuracy of $\pm 2°$. The probable error comes from the unsharpness of the light figure made by the reflection from an etched principal cleavage plane. The resistance of the samples after zone refining were measured at 4.2°K, 88.2°K and 296°K. The results are listed in Table 1. Our result of the resistance ratio $\rho_{4.2°K}/\rho_{296°K}$ is about 5 times the ratio in the lowest resistance crystal reported[1]. From this data only, we can not see how much the crystal was refined by the zone melting but as shown in next section we could get the results for the galvanomagnetic tensors as expected theoretically in very pure samples. Then we believe that the large resistance in zero field of our samples are not due to chemical impurities but due to physical imperfections.

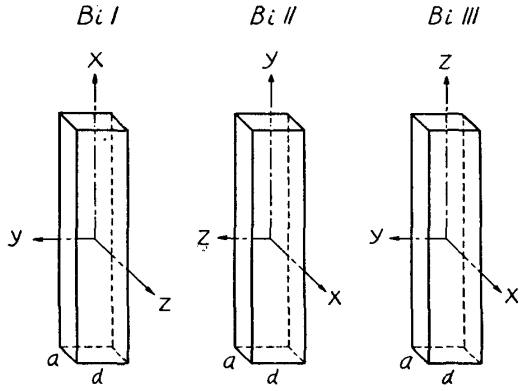

Fig. 1. Crystallographic orientations of samples. x-, z- and y-axis are the binary, the trigonal and the third orthogonal axis respectively.

Table 1. Resistances in zero magnetic field of zone refined bismuth single crystals and the resistance ratio at 4.2°K to at 296°K.

	Resistance at 4.2°K	Resistance at 88.2°K	Resistance at 296°K	$\rho_{4.2°K}/\rho_{296°K}$
Bi I	$1.12\times10^{-6}\Omega$cm	$3.66\times10^{-5}\Omega$cm	$1.16\times10^{-4}\Omega$cm	9.66×10^{-3}
Bi II	$1.48\times10^{-6}\Omega$cm	$3.49\times10^{-5}\Omega$cm	$1.09\times10^{-4}\Omega$cm	1.36×10^{-2}
Bi III	$1.10\times10^{-6}\Omega$cm	$4.02\times10^{-5}\Omega$cm	$1.75\times10^{-4}\Omega$cm	6.29×10^{-3}

b) Apparatus

Resistances and Hall effects were measured by means of a D.C. low voltage potentiometer and a voltage sensitive galvanometer. The magnetic field up to 10 kilo Oersted was provided by a water-cooled electromagnet with a pole gap of 7.7 cm and a diameter of 13 cm. The inhomogeneity of the magnetic field strength over the specimen is less than 0.01%. The electric current strength through samples was usually 0.1 A but in the measurement of the longitudinal effect we used 1 A to increase the accuracy.

Three samples were simultaneously set in a sample holder as shown in Fig. 2. The lucite plate holding each sample can be pulled out from the brass case. The brass case can also be put into the cupper case from its bottom with a lid. Through a hole at one edge of the lid, the lead wires are pulled out and connected

with the outside circuits. This copper case enclosing three samples is immersed in the liquid helium. The magnet can be rotated around the vertical axis. In one measurement the magnet is rotated by 90° or more. After one run of the

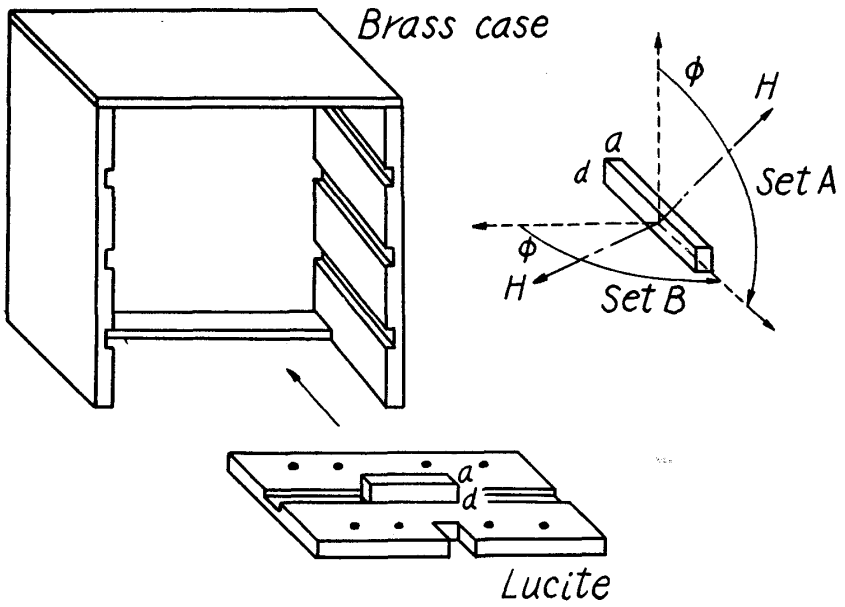

Fig. 2. Sample holder and arrangement of samples.

experiment, we rotate only the brass case by 90° around the horizontal axis, leaving the lucite plates as the first set. Hence in the next run of the experiment, the three samples are rotated by 90° around the long axis of the crystals. At each run of the experiment, the current (only in the case of the longitudinal effect) and the magnetic field are reversed. In the case of the transverse effect, it is checked that the absolute magnitudes of the effect corresponding to the both directions of the current closely coincide to each other. Principally we can obtain all resistivity tensor components in Eq.s (4) by two runs of experiments as shown in Fig. 2. But for the limitation of the time in keeping up the liquid helium, we separated the measurements of the tensors into several runs.

IV. Experimental results

First we tested the Ohm's law on the samples at zero magnetic field. Fig. 3 is a typical example of this measurement. Each point in the figure is the mean value of the voltages at one current direction and the reversed. In the limit of zero current, the voltage in each sample do not tend to zero but to negative value. These may be due to the thermoelectric forces of outside circuits. Actually in zero current through samples, the potentiometer showed negative voltages, its values being almost equal to negative portions of the voltages extrapolated to zero current in the voltage *versus* current curves. Then, this must be corrected in the voltage *versus* current curves to satisfy the Ohm's law. In the measurement of low resistance tensor we used a high current strength to diminish the error arising from this correction.

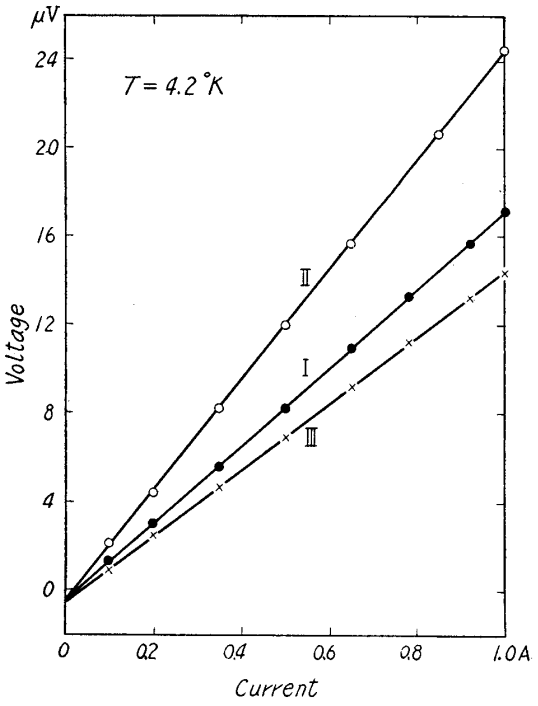

Fig. 3. Voltage *versus* current curves.

In Fig. 4 are shown the longitudinal tensor *versus* H curves. (We use the simple word of 'tensor' in place of 'tensor component'). The reproducibility of $\rho_{xx}(x)$ and $\rho_{yy}(y)$ were fairly satisfactory but not complete. On the other hand that of $\rho_{zz}(z)$ was more unsatisfactory. At weak field these components increase very slightly with magnetic field but at stronger field the magnitudes decrease with the magnetic field. The decrease of $\rho_{zz}(z)$ with the magnetic field is most prominent. The inset in Fig. 4 is the behaviour of $\rho_{zz}(z)$ in *very* weak and moderate fields in which the condition $\omega\tau \lesssim 1$ may be satisfied.

In Fig. 5 are shown other symmetric tensor *versus* H curves. On the contrary to the longitudinal tensors, these curves were well reproducible. All $\rho_{ii}(l)$ $(i \neq l)$ are approximately proportional to $H^{1.7}$.

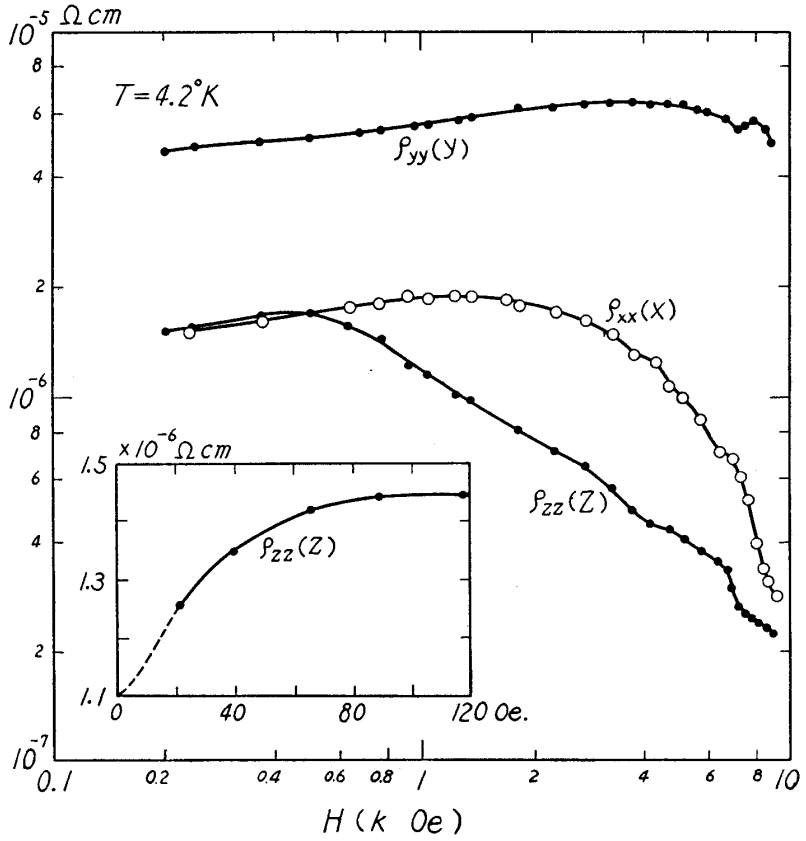

Fig. 4. The longitudinal tensor component *versus* H curves. The inset in the figure is $\rho_{zz}(z)$ in *very* weak and moderate fields.

The anisotropy of the transverse components $\rho_{ii}(l)$ $(i \neq l)$ is considerably smaller than that expected from extreme anisotropy of the energy surfaces of electrons and holes which were deduced from the de Haas-van Alphen effect and the cyclotron resonance. The tensors $\rho^s_{yz}(x)$ and $\rho^s_{yz}(y)$ are characteristic of the bismuth type lattice. Experimental results for these tensors are fairly smaller than those of $\rho_{ii}(l)$ $(i \neq l)$ as is expected, particularly the magnitude of $\rho^s_{yz}(y)$ is smaller by a factor 10^{-2} but considerably larger than the longitudinal tensor $\rho_{ii}(i)$ in strong field. These facts are discussed in the following section in detail.

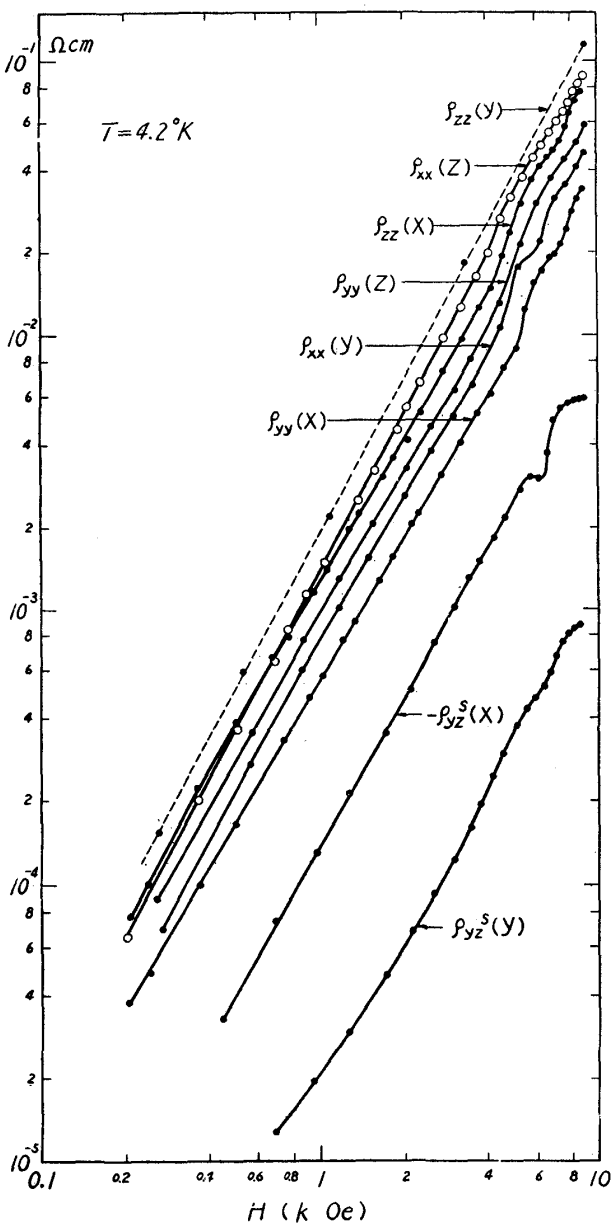

Fig. 5. Symmetric tensor components *versus* H curves.

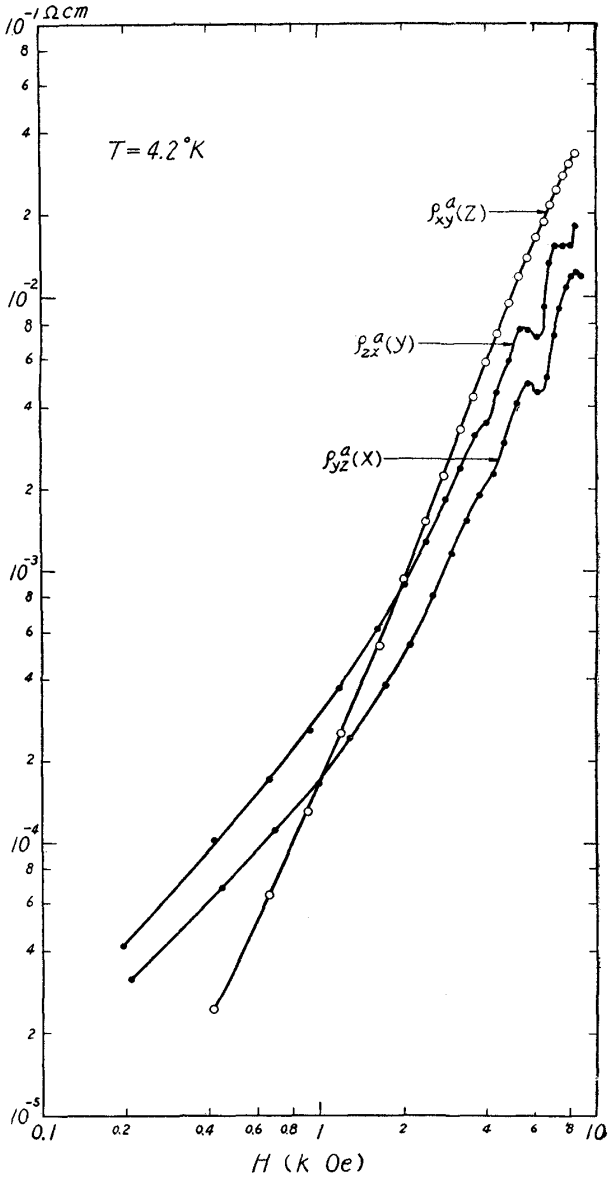

Fig. 6. Antisymmetric tensor components *versus* H curves.

Antisymmetric tensor *versus* H curves are shown in Fig. 6. All these curves are nearly parallel in strong field and $\rho^a_{ik}(l)$ (i, k, l are cyclic of x, y, z) are proportional to $H^{2.1\sim2.4}$. The anisotropy of these tensors is also small and com-

parable order of magnitude to that of the symmetric part $\rho_{ii}(l)$ $(i \neq l)$. The signs of $\rho^a_{yz}(x)$, $\rho^a_{zx}(y)$ and $\rho^a_{xy}(z)$ are all positive, i.e. usual Hall coefficients are all negative.

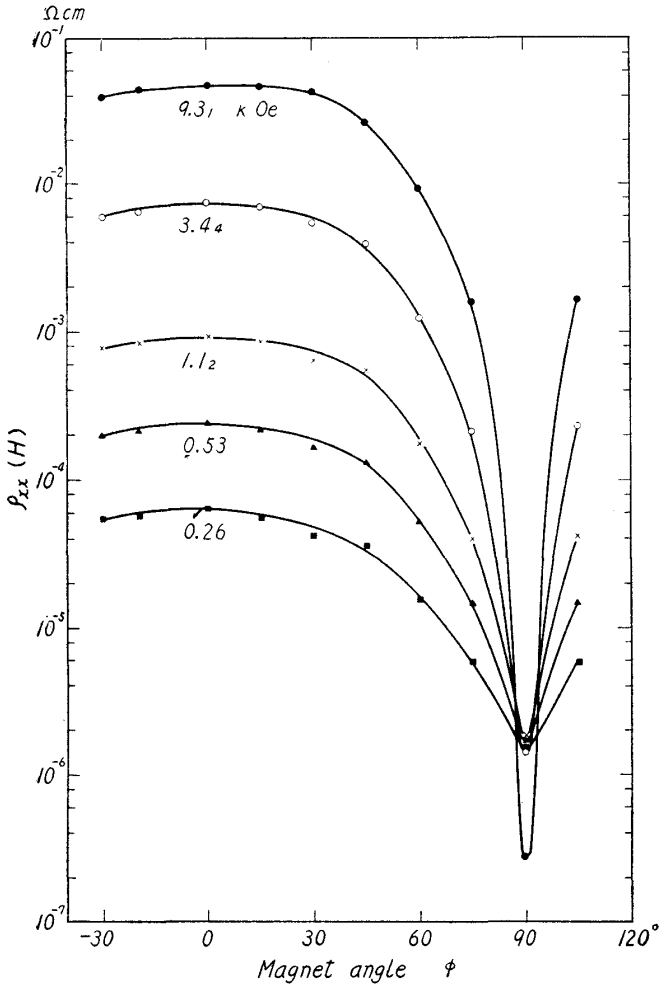

Fig. 7. Symmetric tensor component $\rho_{xx}(H)$ *versus* the angle ϕ of the rotation of the magnet. ϕ is varied about from $\phi=0°$ at $H//y$-axis to $\phi=90°$ at $H//x$-axis. The unit of the numerical values on each figure is the magnetic field strength in kilo Oersted.

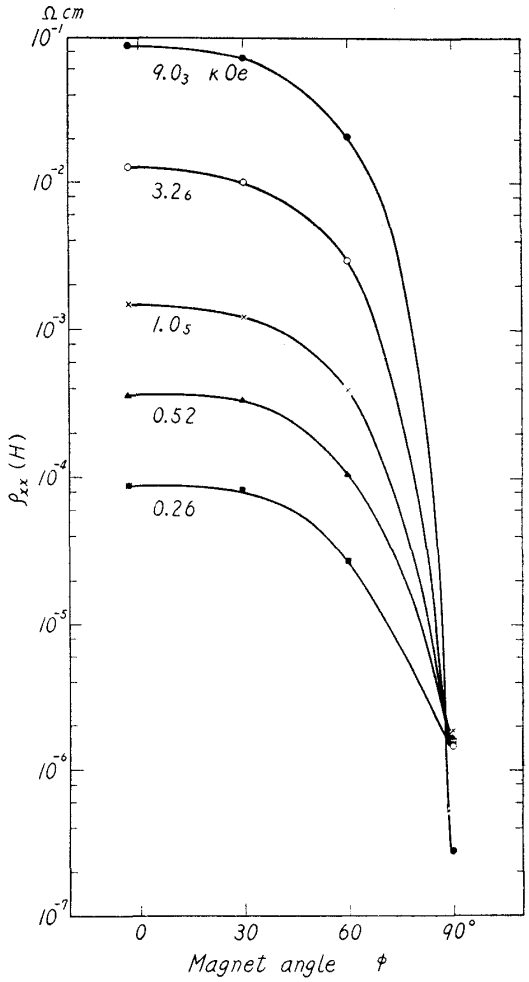

Fig. 8. Symmetric tensor component $\rho_{xx}(H)$ *versus* the angle ϕ of the rotation of the magnet. ϕ is varied about from $\phi=0°$ at $H//z$-axis to $\phi=90°$ at $H//x$-axis.

Fig. 7, 8, 9, 10, 11 and 12 are the plots of $\rho_{ii}(H)$ *versus* the angle of rotation of the magnet with the parameters of the intensity of magnetic field. At zero angle $\rho_{ii}(H)$ becomes purely transverse component and at 90° $\rho_{ii}(H)$ becomes the longitudinal component. Although there is some irregularity because of slight difference of the intensity of magnetic field in each point in each curve, we can conclude that $\rho_{ii}(H)$ varies monotonically with the angle of the magnet except for the possible entrance of a complicated angle dependency related to the de Haas-van Alphen effect. $\rho_{ii}(i)$ is extremely smaller than $\rho_{ii}(l)$ $(i \neq l)$ and with a slight deviation from the longitudinal direction $\rho_{ii}(H)$ increase drastically. Thus

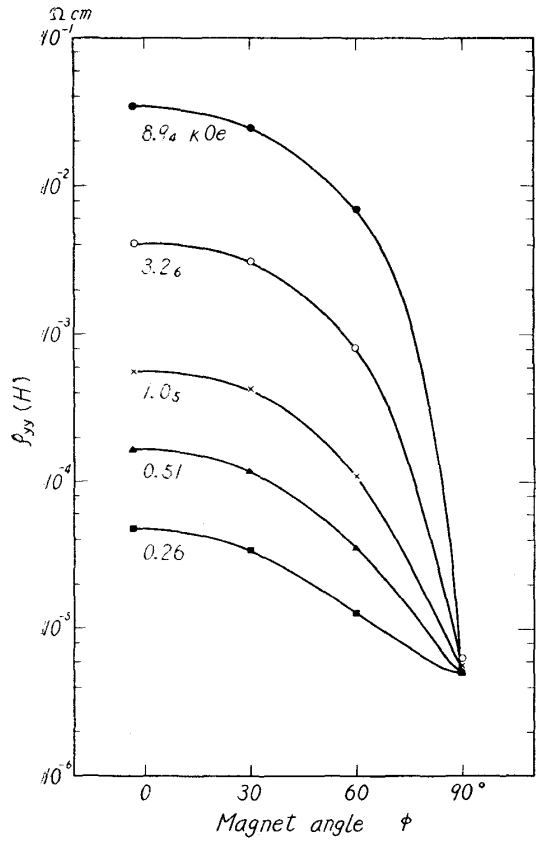

Fig. 9 Symmetric tensor component $\rho_{yy}(H)$ *versus* the angle ϕ of the rotation of the magnet. ϕ is varied about from $\phi=0°$ at $H//x$-axis to $\phi=90°$ at $H//y$-axis.

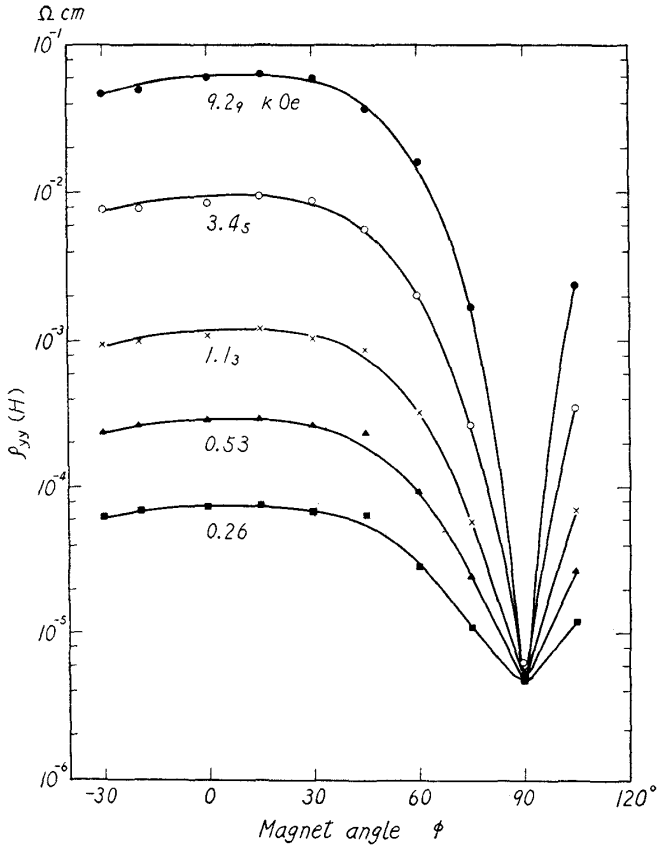

Fig. 10. Symmetric tensor component $\rho_{yy}(H)$ *versus* the angle ϕ of the rotation of the magnet. ϕ is varied about from $\phi=0°$ at $H//z$-axis to $\phi=90°$ at $H//y$-axis.

a slight misalignment of relative position of the magnet or the potential probes to the longer axis of sample can cause such a drastic increase of the voltage between resistance probes in the longitudinal case. In the measurement of the longitudinal effect we paid particular attention in this point but the non-reproducibility of $\rho_{ii}(i)$ as mentioned above may be in some part due to this misalignment of the set.

V. Discussion

Several authors proposed the theories of the galvanomagnetic effect at strong magnetic field[8]. We obtained a flamework of the theory within the limitation of the effective mass approximation, but in order to obtain quantitative predictions we must determine the shape of entire Fermi surface and take account of an anisotropic scattering by static imperfections (or lattice vibration). It is premature to try such calculation for a lack of complete knowledges on energy bands and potentials of lattice defects (or lattice vibration spectrum). Then we see only

(8) P. N. Argyres: Phys. Rev. **109** (1958) 115.
R. Kubo, H. Hasegawa and N. Hashitsume: J. Phys. Soc Japan **14** (1959) 56.

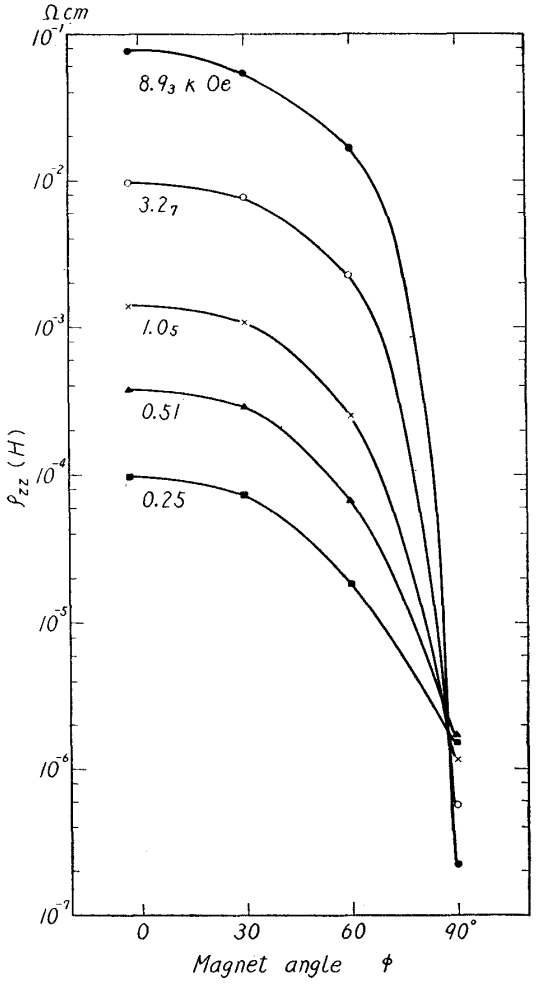

Fig. 11 Symmetric tensor component $\rho_{zz}(H)$ *versus* the angle ϕ of the rotation of the megnet. ϕ is varied about from $\phi=0°$ at $H//x$-axis to $\phi=90°$ at $H//z$-axis.

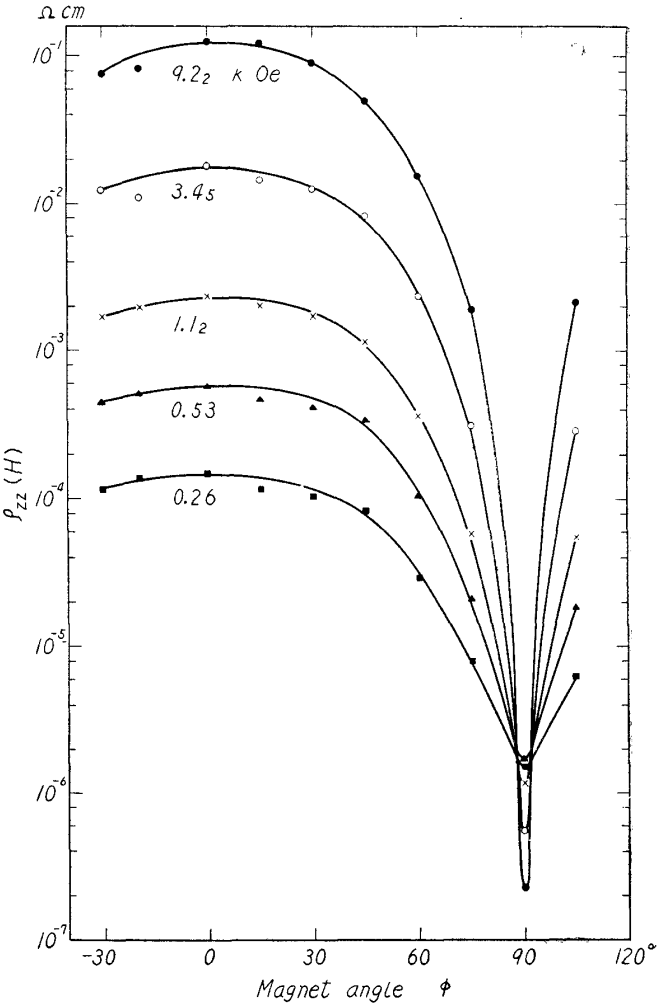

Fig. 12. Symmetric tensor component $\rho_{zz}(H)$ *versus* the angle ϕ of the rotation of the magnet. ϕ is varied about from $\phi=0°$ at $H//y$-axis to $\phi=90°$ at $H//z$--axis.

some theoretical aspect which can be discussed without referring to concrete scattering mechanism.

In view point of principal object for studing monotonic part, we calculate the tensors on the basis of the Bolzmann equation. The neglection of the quantum effect should result to slight disagreement of the magnetic field dependency of the tensors with the experiments. This will not become unsurmounted barrier for understanding of the essential point, because we do not concern here with the behaviour in the quantum limit and the de Haas-van Alphen type oscillation. We would, however, do qualitative discussion of the quantum effect if necessary. For brevity we assume ellipsoidal energy surfaces for both electrons and holes. The electron energy surfaces are taken to be tilted three ellipsoids and the hole energy surface to be single spheroid elongated in the direction of the trigonal

axis.[6),9)-12)] For both electrons and holes we assume energy independent relaxation time tensors $\tau^{(l)}$ which are respectively diagonal in the coordinate system in which each energy surface is diagonal.[13)] The l is the band suffix. In the same system the diagonal mobility tensor $\mu^{(l)}$ is defined with the use of diagonal mass tensor $m^{(l)}$, electric change $e^{(l)}$ and $\tau^{(l)}$ as

$$\mu_i^{(l)} = e^{(l)}\tau_i^{(l)}/m_i^{(l)}. \tag{5}$$

In a magnetic field we calculate partial conductivity tensors in the coordinate system referred to each ellipsoid and transform this to common coordinate system referred to the crystal axes. The calculation under the above assumption is a generalization of that of Abeles and Meiboom[9)] and we write down only the result in the magnetic fields parallel to x-, y- and z- axis:

$H \,//\, x$-axis

$$\sigma(x) = \begin{pmatrix} \sum e^{(l)}n^{(l)}\mu_{xx}^{(l)} \cdot \dfrac{1+(\lambda^{(l)}(x)/\mu_{xx}^{(l)})\,\Gamma^{(l)}(x)^2}{1+\Gamma^{(l)}(x)^2} & 0 & 0 \\ 0 & \sum \dfrac{e^{(l)}n^{(l)}\mu_{yy}^{(l)}}{1+\Gamma^{(l)}(x)^2} & \sum \dfrac{e^{(l)}n^{(l)}\mu_{yz}^{(l)}}{1+\Gamma^{(l)}(x)^2} + \sum \dfrac{(e^{(l)}n^{(l)}c/H_x)\,\Gamma^{(l)}(x)^2}{1+\Gamma^{(l)}(x)^2} \\ 0 & \sum \dfrac{e^{(l)}n^{(l)}\mu_{yz}^{(l)}}{1+\Gamma^{(l)}(x)^2} - \sum \dfrac{(e^{(l)}n^{(l)}c/H_x)\,\Gamma^{(l)}(x)^2}{1+\Gamma^{(l)}(x)^2} & \sum \dfrac{e^{(l)}n^{(l)}\mu_{zz}^{(l)}}{1+\Gamma^{(l)}(x)^2} \end{pmatrix}, \tag{6a}$$

$H//y$-axis

$$\sigma(y) = \begin{pmatrix} \sum \dfrac{e^{(l)}n^{(l)}\mu_{xx}^{(l)}}{1+\Gamma^{(l)}(y)^2} & -\sum \dfrac{(e^{(l)}n^{(l)}c/H_y)\,\Gamma^{(l)}(y)^2}{1+\Gamma^{(l)}(y)^2} \cdot \dfrac{\mu_{xx}^{(l)}\mu_{yz}^{(l)} - \mu_{xy}^{(l)}\mu_{xz}^{(l)}}{\mu_{xx}^{(l)}\mu_{zz}^{(l)} - \mu_{xz}^{(l)2}} & -\sum \dfrac{(e^{(l)}n^{(l)}c/H_y)\,\Gamma^{(l)}(y)^2}{1+\Gamma^{(l)}(y)^2} \\ \sum \dfrac{(e^{(l)}n^{(l)}c/H_y)\,\Gamma^{(l)}(y)^2}{1+\Gamma^{(l)}(y)^2} \cdot \dfrac{\mu_{xx}^{(l)}\mu_{yz}^{(l)} - \mu_{xy}^{(l)}\mu_{xz}^{(l)}}{\mu_{xx}^{(l)}\mu_{zz}^{(l)} - \mu_{xz}^{(l)2}} & \sum e^{(l)}n^{(l)}\mu_{yy}^{(l)} \cdot \dfrac{1+(\lambda^{(l)}(y)/\mu_{yy}^{(l)})\,\Gamma^{(l)}(y)^2}{1+\Gamma^{(l)}(y)^2} & \sum \dfrac{e^{(l)}n^{(l)}\mu_{yz}^{(l)}}{1+\Gamma^{(l)}(y)^2} \\ \sum \dfrac{(e^{(l)}n^{(l)}c/H_y)\,\Gamma^{(l)}(y)^2}{1+\Gamma^{(l)}(y)^2} & \sum \dfrac{e^{(l)}n^{(l)}\mu_{yz}^{(l)}}{1+\Gamma^{(l)}(y)^2} & \sum \dfrac{e^{(l)}n^{(l)}\mu_{zz}^{(l)}}{1+\Gamma^{(l)}(y)^2} \end{pmatrix}, \tag{6b}$$

(9) B. Abeles and S. Meiboom :Phys. Rev. **101** (1956) 544.
(10) B. Lax, K. J. Button, H. J. Zeiger and L. Roth : Phys. Rev. **102** (1956) 715.
(11) S. Mase : J. Phys. Soc. Japan **13** (1958) 434 and **14** (1959) 584.
(12) J. K. Galt, W. A. Yager, F. R. Merritt, B. B. Cetlin and A. D. Brailsford : Phys. Rev. **114** (1959) 1414.
(13) This is a specialization of the treatment for $\tau(k)$ by C. Herring and E. Vogt : Phys. Rev. **101** (1956) 944.

$H//z$-axis

$$\sigma(z)=\begin{pmatrix} \sum \frac{e^{(l)}n^{(l)}\mu_{xx}^{(l)}}{1+\Gamma^{(l)}(z)^2} & \sum \frac{(e^{(l)}n^{(l)}c/H_z)\Gamma^{(l)}(z)^2}{1+\Gamma^{(l)}(z)^2} & 0 \\ -\sum \frac{(e^{(l)}n^{(l)}c/H_z)\Gamma^{(l)}(z)^2}{1+\Gamma^{(l)}(z)^2} & \sum \frac{e^{(l)}n^{(l)}\mu_{yy}^{(l)}}{1+\Gamma^{(l)}(z)^2} & 0 \\ 0 & 0 & \sum e^{(l)}n^{(l)}\mu_{zz}^{(l)}\cdot\frac{1+(\lambda^{(l)}(z)/\mu^{(l)}{}_{zz})\Gamma^{(l)}(z)^2}{1+\Gamma^{(l)}(z)^2} \end{pmatrix}, \tag{6c}$$

where $\Gamma^{(l)}(x)$, $\Gamma^{(l)}(y)$ and $\Gamma^{(l)}(z)$ are dimensionless quantities proportional to H_x, H_y and H_z respectively. $\mu_{ij}^{(l)}$ is ij component of the mobility tensor $\mu^{(l)}$ in the coordinate system referred to the crystal axis and this is expressed by $\mu_i^{(l)}$, the angle $\theta^{(l)}$ of the inclination of one axis of l-th ellipsoid from the trigonal axis, and 120° symmetry. $\lambda^{(l)}(i)$ is some function of $\mu_{ij}^{(l)}$ and $n^{(l)}$ is the number of electrons or holes in l-th band. $\sum$ is the sum of l.

Though above expressions were derived on the special model which we first assumed, these can be applied to any many valley model as far as the energy surfaces are ellipsoids with the trigonal symmetry. Corresponding to each model we can easily calculate $\Gamma^{(l)}(i)$, $\mu_{ij}^{(l)}$ and $\lambda^{(l)}(i)$. We give explicit expression of these quantities in the case of three ellipsoids for electrons (l=1, 2, 3) and one spheroid for holes (l =4). In order to make our study have intimate relation to that of the energy band structure by the cyclotron resonance and the de Haas-van Alphen effect, we rewrite the mobility tensor $\mu_{ij}^{(l)}$ in terms of the isotropic mobility $e^{(\mp)}\tau_0^{(\mp)}/m_0$ and dimensionless quantities ($\gamma_{xx}^{(-)}$, $\gamma_{yy}^{(-)}$, $\gamma_{zz}^{(-)}$, $\gamma_{yz}^{(-)}$) and ($\gamma_{xx}^{(+)}$, $\gamma_{zz}^{(+)}$) as follows,

$$\begin{aligned}
&\gamma_{xx}^{(-)}=\mu_1{}^{(-)}/(e^{(-)}\tau_0{}^{(-)}/m_0),\\
&\gamma_{yy}^{(-)}=(\cos^2\theta\cdot\mu_2{}^{(-)}+\sin^2\theta\cdot\mu_3{}^{(-)})/(e^{(-)}\tau_0{}^{(-)}/m_0),\\
&\gamma_{zz}^{(-)}=(\sin^2\theta\cdot\mu_2{}^{(-)}+\cos^2\theta\cdot\mu_3{}^{(-)})/(e^{(-)}\tau_0{}^{(-)}/m_0),\\
&\gamma_{yz}^{(-)}=\sin\theta\cos\theta\cdot(\mu_3{}^{(-)}-\mu_2{}^{(-)})/(e^{(-)}\tau_0{}^{(-)}/m_0),\\
&\gamma_{xx}^{(+)}=\mu_1{}^{(+)}/(e^{(+)}\tau_0{}^{(+)}/m_0),\\
&\gamma_{zz}^{(+)}=\mu_3{}^{(+)}/(e^{(+)}\tau_0{}^{(+)}/m_0).
\end{aligned} \tag{7}$$

Four parameters $\mu_1{}^{(-)}$, $\mu_2{}^{(-)}$, $\mu_3{}^{(-)}$ and θ for electrons are replaced by $(e^{(-)}\tau_0{}^{(-)}/m_0)$, $\gamma_{xx}^{(-)}/\gamma_{zz}^{(-)}$, $\gamma_{yy}^{(-)}/\gamma_{zz}^{(-)}$ and $\gamma_{yz}^{(-)}/\gamma_{zz}^{(-)}$. Similarly $\mu_1{}^{(+)}$ and $\mu_3{}^{(+)}$ for holes are replaced by $e^{(+)}\tau_0{}^{(+)}/m_0$ and $\gamma_{xx}^{(+)}/\gamma_{zz}^{(+)}$. $\mu_{ij}^{(l)}$ of each band is shown in Table 2. In terms of $\gamma_{ij}^{(\pm)}$, $\Gamma^{(l)}(i)$ and $\lambda^{(l)}(i)$ are given by

$$\begin{aligned}
&\Gamma^{(1)}(x)^2=\mu_2{}^{(-)}\mu_3{}^{(-)}(H_x^2/c^2)=(\gamma_{yy}^{(-)}\gamma_{zz}^{(-)}-\gamma_{yz}^{(-)2})(\omega_0\tau_0{}^{(-)})^2,\\
&\Gamma^{(2)}(x)^2=\Gamma^{(3)}(x)^2=(\mu_2{}^{(-)}\mu_3{}^{(-)}+3\cos^2\theta\cdot\mu_1{}^{(-)}\mu_3{}^{(-)}+3\sin^2\theta\cdot\mu_1{}^{(-)}\mu_2{}^{(-)})(H_x^2/4c^2)\\
&\qquad=1/4\cdot\{(\gamma_{yy}^{(-)}\gamma_{zz}^{(-)}-\gamma_{yz}^{(-)2})+3\gamma_{xx}^{(-)}\gamma_{zz}^{(-)}\}(\omega_0\tau_0{}^{(-)})^2,
\end{aligned} \tag{8a}$$

$$\left.\begin{aligned}
&\Gamma^{(4)}(x)^2=\mu_1^{(+)}\mu_3^{(+)}(H_x^2/c^2)=(\gamma_{xx}^{(+)}\gamma_{zz}^{(+)})(\omega_0\tau_0^{(+)})^2,\\
&\lambda^{(l)}(x)=\mu_{xx}^{(l)}-(\mu_{yy}^{(l)}\mu_{xz}^{(l)2}+\mu_{zz}^{(l)}\mu_{xy}^{(l)2}-2\mu_{xy}^{(l)}\mu_{yz}^{(l)}\mu_{xz}^{(l)})/(\mu_{yy}^{(l)}\mu_{zz}^{(l)}-\mu_{yz}^{(l)2}),
\end{aligned}\right\}$$

$$\left.\begin{aligned}
&\Gamma^{(1)}(y)^2=(\cos^2\theta\cdot\mu_1^{(-)}\mu_3^{(-)}+\sin^2\theta\cdot\mu_1^{(-)}\mu_2^{(-)})(H^2{}_y/c^2)=(\gamma_{xx}^{(-)}\gamma_{zz}^{(-)})(\omega_0\tau_0^{(-)})^2,\\
&\Gamma^{(2)}(y)^2=\Gamma^{(3)}(y)^2=(3\mu_2^{(-)}\mu_3^{(-)}+\cos^2\theta\cdot\mu_1^{(-)}\mu_3^{(-)}+\sin^2\theta\cdot\mu_1^{(-)}\mu_2^{(-)})(H_y^2/4c^2)\\
&\qquad=1/4\cdot\{3(\gamma_{yy}^{(-)}\gamma_{zz}^{(-)}-\gamma_{yz}^{(-)2})+\gamma_{xx}^{(-)}\gamma_{zz}^{(-)}\}(\omega_0\tau_0^{(-)})^2,\\
&\Gamma^{(4)}(y)^2=\mu_1^{(+)}\mu_3^{(+)}(H_y^2/c^2)=(\gamma_{xx}^{(+)}\gamma_{zz}^{(+)})(\omega_0\tau_0^{(+)})^2,\\
&\lambda^{(l)}(y)=\mu_{yy}^{(l)}-(\mu_{zz}^{(l)}\mu_{xy}^{(l)2}+\mu_{xx}^{(l)}\mu_{yz}^{(l)2}-2\mu_{xy}^{(l)}\mu_{yz}^{(l)}\mu_{xz}^{(l)})/(\mu_{xx}^{(l)}\mu_{zz}^{(l)}-\mu_{xz}^{(l)2}),
\end{aligned}\right\}\quad(8b)$$

$$\left.\begin{aligned}
&\Gamma^{(1)}(z)^2=\Gamma^{(2)}(z)^2=\Gamma^{(3)}(z)^2=(\cos^2\theta\cdot\mu_1^{(-)}\mu_2^{(-)}+\sin^2\theta\cdot\mu_1^{(-)}\mu_3^{(-)})(H_z^2/c^2)\\
&\qquad=(\gamma_{xx}^{(-)}\gamma_{yy}^{(-)})(\omega_0\tau_0^{(-)})^2,\\
&\Gamma^{(4)}(z)^2=\mu_1^{(+)2}(H_z^2/c^2)=\gamma_{xx}^{(+)2}(\omega_0\tau_0^{(+)})^2,\\
&\lambda^{(l)}(z)=\mu_{zz}^{(l)}-(\mu_{xx}^{(l)}\mu_{yz}^{(l)2}+\mu_{yy}^{(l)}\mu_{xz}^{(l)2}-2\mu_{xy}^{(l)}\mu_{yz}^{(l)}\mu_{zx}^{(l)})/(\mu_{xx}^{(l)}\mu_{yy}^{(l)}-\mu_{xy}^{(l)2}).
\end{aligned}\right\}\quad(8c)$$

Table 2. Mobility tensor components in common coordinate system.

Band	$\mu_{xx}^{(l)}/(e^{(l)}\tau_0^{(l)}/m_0)$	$\mu_{yy}^{(l)}/(e^{(l)}\tau_0^{(l)}/m_0)$	$\mu_{zz}^{(l)}/(e^{(l)}\tau_0^{(l)}/m_0)$	$\mu_{xy}^{(l)}/(e^{(l)}\tau_0^{(l)}/m_0)$	$\mu_{xz}^{(l)}/(e^{(l)}\tau_0^{(l)}/m_0)$	$\mu_{yz}^{(l)}/(e^{(l)}\tau_0^{(l)}/m_0)$
1	$\gamma_{xx}^{(-)}$	$\gamma_{yy}^{(-)}$	$\gamma_{zz}^{(-)}$	0	0	$\gamma_{yz}^{(-)}$
2	$\frac{1}{4}(\gamma_{xx}^{(-)}+3\gamma_{yy}^{(-)})$	$\frac{1}{4}(3\gamma_{xx}^{(-)}+\gamma_{yy}^{(-)})$	$\gamma_{zz}^{(-)}$	$\frac{\sqrt{3}}{4}(\gamma_{xx}^{(-)}-\gamma_{yy}^{(-)})$	$\frac{\sqrt{3}}{2}\gamma_{yz}^{(-)}$	$-\frac{1}{2}\gamma_{yz}^{(-)}$
3	$\frac{1}{4}(\gamma_{xx}^{(-)}+3\gamma_{yy}^{(-)})$	$\frac{1}{4}(3\gamma_{xx}^{(-)}+\gamma_{yy}^{(-)})$	$\gamma_{zz}^{(-)}$	$-\frac{\sqrt{3}}{4}(\gamma_{xx}^{(-)}-\gamma_{yy}^{(-)})$	$-\frac{\sqrt{3}}{2}\gamma_{yz}^{(-)}$	$-\frac{1}{2}\gamma_{yz}^{(-)}$
4	$\gamma_{xx}^{(+)}$	$\gamma_{xx}^{(+)}$	$\gamma_{zz}^{(+)}$	0	0	0

In the case of the isotropic scattering, $\gamma_{ij}^{(\mp)}$ is reduced to the effective mass parameters $\alpha_{ij}^{(\mp)}$ in the ellipsoidal energy surfaces defined by

$$\varepsilon^{(1)}(P)=\frac{1}{2m_0}(\alpha_{xx}^{(-)}P_x^2+\alpha_{yy}^{(-)}P_y^2+\alpha_{zz}^{(-)}P_z^2+2\alpha_{yz}^{(-)}P_yP_z),\quad(9a)$$

$$\varepsilon^{(4)}(P)=-\frac{1}{2m_0}(\alpha_{xx}^{(+)}P_x^2+\alpha_{xx}^{(+)}P_y^2+\alpha_{zz}^{(+)}P_z^2).\quad(9b)$$

Then $\Gamma^{(l)}(i)$ is reduced to the product of the cyclotron frequency $\omega^{(l)}(i)$ and the isotropic relaxation time $\tau_0^{(l)}$. On the other hand, $\lambda^{(l)}(i)$ is related to the unquantized energy component $\varepsilon_{\parallel}^{(l)}$ parallel to the magnetic field H_i by the formula $\varepsilon_{\parallel}^{(l)}=\hbar^2k_i^2/2m_0\cdot\lambda^{(l)}(i)/(e^{(l)}\tau_0^{(l)}/m_0)$. In fact the expression of Eq.s (6) is designed to be continued naturally on the quantum mechanical calculation which is now progressing.

There are two ways when comparing the experimental results with a theory.

One is to compare theoretical conductivity tensor with experimental conductivity tensor σ given by inverse tensor of ρ. This method can be adopted only when all resistivity tensor components are measured consistently. The other is to compare theoretical resistivity tensor σ^{-1} with experimental ρ. When the calculation of σ is performed orthodoxically with no parameter, the latter method is well suited. Unfortunately neither case is corresponded to our result. We consider, however, that the latter is better in the present case.

The resistivity tensor ρ is given as follows:

$H//x$-axis

$$\rho(x)=\begin{pmatrix} 1/\sigma_{xx} & 0 & 0 \\ 0 & \sigma_{zz}/\Delta(x) & -\sigma^s_{yz}/\Delta(x)-\sigma^a_{yz}/\Delta(x) \\ 0 & -\sigma^s_{yz}/\Delta(x)+\sigma^a_{yz}/\Delta(x) & \sigma_{yy}/\Delta(x) \end{pmatrix}, \tag{10a}$$

where $\Delta(x)=\sigma_{yy}\sigma_{zz}+\sigma^{a\,2}_{yz}-\sigma^{s\,2}_{yz}$,

$H//y$-axis

$$\rho(y)=\frac{1}{\det\sigma}\begin{pmatrix} \sigma_{yy}\sigma_{zz}-\sigma^{s\,2}_{yz} & -\sigma_{zz}\sigma^a_{xy}-\sigma^s_{yz}\sigma^a_{zx} & \sigma_{yy}\sigma^a_{zx}+\sigma^s_{yz}\sigma^a_{xy} \\ \sigma_{zz}\sigma^a_{xy}+\sigma^s_{yz}\sigma^a_{zx} & \sigma_{xx}\sigma_{zz}+\sigma^{a\,2}_{zx} & -\sigma_{xx}\sigma^s_{yz}+\sigma^a_{xy}\sigma^a_{zx} \\ -\sigma_{yy}\sigma^a_{zx}-\sigma^s_{yz}\sigma^a_{xy} & -\sigma_{xx}\sigma^s_{yz}+\sigma^a_{xy}\sigma^a_{zx} & \sigma_{xx}\sigma_{yy}+\sigma^{a\,2}_{xy} \end{pmatrix}, \tag{10b}$$

$H//z$-axis

$$\rho(z)=\begin{pmatrix} \sigma_{xx}/\Delta(z) & -\sigma^a_{xy}/\Delta(z) & 0 \\ \sigma^a_{xy}/\Delta(z) & \sigma_{xx}/\Delta(z) & 0 \\ 0 & 0 & 1/\sigma_{zz} \end{pmatrix}, \tag{10c}$$

where $\Delta(z)=\sigma^2_{xx}+\sigma^{a\,2}_{xy}$.

Of course these are in accordance with the phenomenological results in § 2.

a) Antisymmetric tensors

In the case $H//z$-axis, the resistivity tensor has the same character as in the case of an isotropic energy surface. First we discuss of this simple case somewhat in detail. The tensor $\sigma^a_{xy}(z)$ is rewrited in

$$\sigma^a_{xy}(z)=\sum\frac{e^{(l)}n^{(l)}c}{H_z}-\sum\frac{e^{(l)}n^{(l)}c}{H_z}\cdot\frac{1}{1+\Gamma^{(l)}(z)^2}. \tag{11}$$

The ratio of the second term of $\sigma^a_{xy}(z)$ to $\sigma_{xx}(z)$ is the order of $1/\Gamma(z)$, because

$$\frac{(e^{(l)}n^{(l)}c/H_z)}{e^{(l)}n^{(l)}\mu^{(l)}_{xx}}=\frac{c}{H_z\mu^{(l)}_{xx}}\cong\frac{1}{\Gamma^{(l)}(z)}.$$

Then we may neglect the second term of $\sigma^a_{xy}(z)$ in a strong field. In fact we can not explain the field dependency of $\rho^a_{xy}(z)$ by this second term. The first term of $\sigma^a_{xy}(z)$ is rewrited as

$$\sum \frac{e^{(l)}n^{(l)}c}{H_z} = -\frac{en_0c}{H_z}\frac{\Delta n}{n_0} \qquad (e>0), \tag{12}$$

where $n_0=(n^{(-)}+n^{(+)})/2$ and $\Delta n=n^{(-)}-n^{(+)}$. From the experimental fact that $\rho^a_{xy}(z)\sim 1/2\cdot\rho_{xx}(z)$ at $H\sim 8$ kilo Oersted, we must assume that

$$\frac{\rho^a_{xy}(z)}{\rho_{xx}(z)} = -\frac{\sigma^a_{xy}(z)}{\sigma_{xx}(z)} \sim \frac{(en_0c/H_z)(\Delta n/n_0)}{e^{(k)}n^{(k)}\mu^{(k)}_{xx}/\Gamma^{(k)}(z)^2} \sim \Gamma^{(k)}(z)\frac{\Delta n}{n_0} \lesssim 1,$$

i.e.

$$\frac{\Delta n}{n_0} \lesssim \frac{1}{\Gamma^{(k)}(z)}\,. \tag{13}$$

Since $\Gamma^{(k)}(z)$ is estimated to the order of 100~1000 at $H\sim 8$ kilo Oersted and 4.2°K, very slight excess of electrons is demanded to obtain the agreement with the experiment. The field dependency of $\rho^a_{xy}(z)$ becomes

$$\rho^a_{xy}(z) \propto \frac{\Delta n/H_z}{(A\nu_s^2/H_z^4)+(B(\Delta n)^2/H_z^2)} = \frac{\Delta n\cdot H_z^3}{A\nu_s^2+B(\Delta n)^2H_z^2} \qquad (A\nu_s^2>B(\Delta n)^2H_z^2), \tag{14}$$

where ν_s is the number of scattering centres. The other antisymmetric tensor components $\rho^a_{yz}(x)$ and $\rho^a_{zx}(y)$ should have also the same sign and similar field dependency as $\rho^a_{xy}(z)$ in the classical approximation.

In an impure crystal such as $\Delta n\gtrsim n_0/10$ and in a pure crystal but in very strong field such as $\Delta n/n_0\cdot\Gamma^{(k)}(z)\gg 1$, $-\sigma^a_{xy}(z)$ becomes larger than $\sigma_{xx}(z)$ and we obtain the resistivity tensor

$$\rho(z)=\begin{pmatrix} \sigma_{xx}/\sigma^{a\,2}_{xy} & -1/\sigma^a_{xy} & 0 \\ 1/\sigma^a_{xy} & \sigma_{xx}/\sigma^{a\,2}_{xy} & 0 \\ 0 & 0 & 1/\sigma_{zz} \end{pmatrix}. \tag{15}$$

In the former case the tensor components become as follows

$$\rho^a_{xy}(z)\sim H_z/\Delta nec\,, \qquad \rho_{xx}(z)\sim\rho^0_{xx}\,, \qquad \rho_{zz}(z)\sim\rho^0_{zz}\,. \tag{16}$$

Antisymmetric tensor divided by H, $-\rho^a_{ik}(l)/H_l$ (i, k, l are cyclic of x, y, z), is related to usual Hall coefficient and in impure crystals the coefficient becomes a constant independent of the magnetic field. These results are characteristic in monovalent metals. On the other hand the latter case is related to the occurence of the saturation in very strong field. In the present purity of samples, the saturation field should be much stronger than our maximum field. Moreover the behaviour in such strong field is essentially quantum mechanical.

Our experimental value of the monotonic part of $\rho^a_{ik}(l)$ is proportional to $H^{2.1\sim2.4}$. This result is comparable order of magnitude to that of Okada[5] ($\rho^a_{xy}(z)$, $\rho^a_{yz}(x)\propto H^{2.0\sim2.1}$). The absolute magnitude of our tensors $\rho^a_{xy}(z)$ and $\rho^a_{yz}(x)$ are 8 and 3 times respectively the corresponding tensors by Okada. (He found, however, nearly no anisotropy in $\rho^a_{xy}(z)$ and $\rho^a_{yz}(x)$). In the present theory the difference

of the absolute magnitudes should be attributed to the differences in Δn and ν_s, since

$$\rho^a_{xy}(z) \sim \frac{\sigma^a_{xy}(z)}{\sigma_{xx}(x)^2} \propto \frac{\Delta n H_z^3}{\nu_s^2} , \tag{17a}$$

$$\rho^a_{yz}(x) \sim -\frac{\sigma^a_{yz}(x)}{\sigma_{yy}(x)\sigma_{zz}(x)} \propto \frac{\Delta n \cdot H_x^3}{\nu_s^2} . \tag{17b}$$

The experimental result of the field dependency of $\rho^a_{ik}(l)$ is much similar to the theoretical prediction in a pure crystal rather than that in an impure crystal. The discrepancy might be got rid of by taking account of the quantum effect in the calculation of the symmetric conductivity tensors.

At first sight it seems that we can explain nicely both the absolute value and the field dependency of the antisymmetric tensor in the above manner. There are, however, many doubts to this explanation. First we have not any natural explanation why the number of electrons always exceeds that of holes very slightly in highly zone-refined crystals, as shown by negative Hall coefficients obtained by Connel-Marcus, Okada and us. Secondly the absolute magnitude of $\rho^a_{ik}(l)$ increases largely with the increase of chemical purity of the sample containing some physical imperfections (this means that Δn becomes very small but ν_s is the same order of magnitude). The dependency of the amplitude of the periodic part on the purity of samples is also unexplained by the above scheme[3]. These facts throw a doubt to the usual theory based on the effective mass approximation. We would discuss of this further in the following section b).

Finaly we point out that the result of our rough analysis for the periodic part seems to be in an accordance with those of the previous workers, though our analysis is only a check for the crystallographic orientations.

b) Symmetric tensors

We begin with the longitudinal effect. According to the present theory the longitudinal tensor $\rho_{zz}(z)$ is given by

$$\rho_{zz}(z) = (\sum e^{(l)} n^{(l)} \mu^{(l)}_{zz})^{-1} + \rho_{zz,zz} H_z^2 + \cdots \qquad \text{(in } \textit{very} \text{ weak field)}, \tag{18a}$$

$$\rho^{\infty}_{zz}(z) = (\sum e^{(l)} n^{(l)} \lambda^{(l)}(z))^{-1} \qquad (H_z \to \infty). \tag{18b}$$

Since $\lambda^{(l)}(z) \leq \mu^{(l)}_{zz}$, we can say that $\rho_{zz}(z)$ increases monotonically from ρ^0_{zz} to the saturation value $\rho^{\infty}_{zz}(z)$. In the special model with $\theta=0$, we obtain $\lambda^{(l)}(z) = \mu^{(l)}_{zz}$ and the longitudinal magnetoresistance disappears, i.e. $\rho_{zz}(z) = \rho^0_{zz}$. The experiment is not the case. On the field dependency of $\rho_{xx}(x)$ and $\rho_{yy}(y)$, similar argument can be made. In the latter case, however, $\lambda^{(l)}(x) < \mu^{(l)}_{xx}$ and $\lambda^{(l)}(y) < \mu^{(l)}_{yy}$ even if $\theta=0$.

While, except the second run for $\rho_{zz}(z)$ (the inset in Fig. 4), each component $\rho_{ii}(i)$ in the lowest magnetic field in Fig. 4 is much larger than the residual resistance ρ^0_{ii}. This difference is due to the fact that at the liquid helium temperature the condition Γ (or $\omega\tau$) >1 is necessarily satisfied in presence of the lowest field and the solution is in saturation region of that of the Boltzmann equation.

Thus at lower magnetic field as Γ (or $\omega\tau$)$\sim$1, the longitudinal tensor should change the magnitude from the Boltzmann case to the higher field value. This change from *very* weak to stronger field region is illustrated in the inset in Fig. 4. Afterward, due to the quantum effect the tensor may increase slowly with the magnetic field, if the crystal is free from the slip surfaces or other boundary surfaces. In our results all components increase slightly in the weak field, except second run for $\rho_{zz}(z)$, but in the stronger field each $\rho_{ii}(i)$ begins to decrease. This negative magnetoresistance is undesirable effect for the present purpose. Similar effect was found by Steele[14] ($\rho_{xx}(x)$ and $\rho_{yy}(y)$ in antimony), Babiskin[4] ($\rho_{zz}(z)$) and Okada[5] ($\rho_{xx}(x)$). The fact that the values of ρ^0_{xx} and ρ^0_{yy} at 4.2°K measured outside the magnet are not in accordance shows the existence of the boundary effect. From the crystal symmetry alone, ρ^0_{xx} and ρ^0_{yy} should be in accordance and in fact as shown as Bi I and Bi II in Table 1, these are nearly equal at liquid air and room temperatures at which the boundary effect is negligible. Then this negative magnetoresistance is related partly to inner boundary effects. In our data on this anomalous magnetoresistance it does not exist any definite regarlarity such that we can attribute this to, for example, the principal cleavage planes. Alekseevskii et al[15] attributed this negative magnetoresistance to the end effect due to a stray current and a nonparallelism of potential electrodes. Since our three samples are set in almost the same situation, the end effect is not primarily concerned but the boundary effect and very slight misalignment are so.

Babiskin[4] measured the longitudinal tensors $\rho_{xx}(x)$ and $\rho_{zz}(z)$ up to 60 kilo Oersted and found that $\rho_{zz}(z)$ is nearly constant up to 10 kilo Oersted but at stronger fields $\rho_{zz}(z)$ increases quadratically with the magnetic field. This quadratic dependency is characteristic for the transverse tensor as seen from Fig. 5. Since the transverse component is greater than the longitudinal component by a factor larger than 10^4 at $H>10$ kilo Oersted, only slight misalignment of the potential probes and the magnetic field relative to the referred axis could cause such dependency due to the transverse component. Non-zero value of $\rho_{yx}(x)$ found by him should vanish from the crystal symmetry and reciprocal relation alone and this may be partly related to the misalignment mentioned above. Considerable increase of his curve I of $\rho_{xx}(x)$ in wide range of field is also essentially different from ours.

The result that the transverse components are extremely larger than the longitudinal components arises from the cancellation of the antisymmetric conductivity tensor due to closely equal number of electrons and holes, as we have made clear in the section a). The theoretical field dependency of diagonal transverse tensor, for example $\rho_{xx}(z)$, in strong fields is

$$\rho_{xx}(z) \propto \frac{\nu_s/H_z^2}{(A\nu_s^2/H_z^4)+(B(\Delta n)^2/H_z^2)} = \frac{\nu_s H_z^2}{A\nu_s^2+B(\Delta n)^2 H_z^2}, \qquad (A\nu_s^2 > B(\Delta n)^2 H_z^2). \quad (19)$$

(14) M. C. Steele: Phys. Rev. **97** (1955) 1720; *Conference de Physique des Basses Temperatures*, Paris (1955) 415.

(15) N. E. Alekseevskii, N. B. Brandt, and T. I. Kostina: Sov. Phys. JETP **7** (1958) 924.

In a rough approximation $\rho_{xx}(z)$ becomes proportional to H_z^2/ν_s. On the other components $\rho_{ii}(l)$ $(i \neq l)$, we obtain similar result though there is some complexity due to the appearance of unfamilar type of tensor components in the cases of the field parallel to x- and y-axis.

On the field dependency of the monotonic part, Alers and Webber[1] found that $\rho_{zz}(y) \propto H^{1.66}$ and Okada[5] found that $\rho_{xx}(z)$ and $\rho_{zz}(x)$ are both proportional to $H^{1.6}$. Our result $\rho_{ii}(l) \propto H^{1.7}$ $(i \neq l)$ is comparable order to theirs. The absolute value of $\rho_{xx}(z)$ and $\rho_{zz}(x)$ are about 3.6 and 2.7 times the corresponding tensors by Okada. This is expected from the fact that the residual resistances $\overset{0}{\rho}_{xx}$ and $\overset{0}{\rho}_{zz}$ of our samples are about 1/1.4 and 1/2.4 times respectively the correspondings by Okada ($\overset{0}{\rho}_{xx} \sim 1.6 \times 10^{-6}$ Ωcm and $\rho_{zz} \sim 2.6 \times 10^{-6}$ Ωcm), i.e. that ν_s of our samples is smaller.

The disagreement of theoretical field dependency with experiments should be got rid of by taking account of the quantum effect. The comparatively small anisotropy of $\rho_{ii}(l)$ $(i \neq l)$ should be noted. Analyses of the de Haas-van Alphen type oscillation of susceptibility and galvanomagnetic tensors and also of the cyclotron resonance give the values of α_{ij} of electrons and holes (Table 3). Though we can not regard these values to be decisive in the present stage of studies, we temporarily use these and further we assume an isotropic scattering time $\tau_0^{(-)} = \tau_0^{(+)}$ for both electrons and holes. Under these assumptions and with a rough approximation $\rho_{ii}(l) \sim 1/\sigma_{ii}(l)$, theoretical values of $\rho_{ii}(l)$ yield

$$\begin{aligned} &\rho_{yy}(x) \sim 1.07\bar{\rho}, \quad &&\rho_{zz}(x) \sim 1.50\bar{\rho}, \quad &&\rho_{yz}^s(x) \sim -0.22\bar{\rho}, \\ &\rho_{xx}(y) \sim 1.08\bar{\rho}, \quad &&\rho_{zz}(y) \sim 10.4\bar{\rho}, \quad &&\rho_{xx}(z) \sim 2.41\bar{\rho}, \end{aligned} \tag{20}$$

for Galt et al's values[11] of α_{ij} for electrons and holes, where $\bar{\rho} = (n_0 e^2 \tau_0/m_0)^{-1} \cdot \omega_0^2 \tau_0^2$. For comparison there is shown the value of $\rho_{yz}^s(x)$ calculated by the approximate formula $\rho_{yz}^s(x) \sim -\sigma_{yz}^s(x)/\sigma_{yy}(x)\,\sigma_{zz}(x)$ and with positive $\alpha_{yz}^{(-)}$. This anisotropy is almost along the same line with the experiment. Theoretical largest anisotropy ratio $\rho_{zz}(y)/\rho_{yy}(x) \sim 9.7$ is, however, considerably larger than that of experiment. Even if we take account of possible errors for the values of α_{ij} and for the experimental values of $\rho_{ii}(l)$, this discrepancy may not be got rid of. It seems that this result shows the importance of anisotropic scattering or a failure of the usual effective mass theory. Unfortunately our experimental result does not satisfy the symmetry relation $\rho_{xx}(z) = \rho_{yy}(z)$ required from the phenomenological

Table 3. Effective mass parameters $\alpha_{ij}^{(\mp)}$ from the experiments by Galt et al[a] and Shoenberg[b].

	$\alpha_{xx}^{(\mp)}$	$\alpha_{yy}^{(\mp)}$	$\alpha_{zz}^{(\mp)}$	$\alpha_{yz}^{(\mp)}$
Electron[a]	114	1.46	114	$\pm$10.1
Hole[a]	14.7	14.7	1.09	0
Electron[b]	417	0.8	40	4

theory because of probable existence of the boundary effect in the transverse components as well as in the longitudinal components. So we could not use our data for examining quantitatively the intrinsic properties of bismuth, i.e. the anisotropic energy surfaces of electrons and holes, and the anisotropic scattering by random lattice defects.

Finally we note of very large difference in the order of magnitudes of $\rho_{yy}(y)$, $\rho^s_{yz}(y)$ and $\rho_{zz}(y)$. At $H\sim 8$ kilo Oersted, the experimental ratio of these quantities is

$$\rho_{yy}(y) : \rho^s_{yz}(y) : \rho_{zz}(y) \sim 1 : 100 : 10000 \quad (H\sim 8 \text{ kOe.}). \tag{21}$$

This difference, of course, can be explained by Eq.s (10). $\rho^s_{yz}(y)$ is given by

$$\rho^s_{yz}(y) = (-\sigma_{xx}(y)\sigma^s_{yz}(y) + \sigma^a_{xy}(y)\sigma^a_{zx}(y))/\det\sigma(y) \ .$$

In the numerator, the first term proportional to $1/H_y^4$ is clearly very smaller than the second term proportional to $1/H_y^2$. While the leading term of the denominator is proportional to $1/H_y^4$. Then $\rho^s_{yz}(y)$ is approximately proportional to H_y^2 in the classical theory. As was expressed in the section a), $\Delta n/n_0$ is estimated to the order of $1/\Gamma$ at $H\sim 8$ kilo Oersted. We assume $\Delta n/n_0 \sim 1/1000$. Then we have

$$\sigma^a_{zx}(y) = -\frac{en_0c}{H_y}\cdot\frac{\Delta n}{n_0} \sim -\frac{1}{1000}\frac{en_0c}{H_y} \ . \tag{22}$$

On the other hand $\sigma^a_{xy}(y)$ is estimated by using the experimental data for $\alpha^{(I)}_{ij}$. We have

$$\sigma^a_{xy}(y) \sim -\frac{1}{4}\frac{en_0c}{H_y} \tag{23}$$

for positive $\alpha^{(-)}_{yz}$. Then we get positive sign for $\rho^s_{yz}(y)$ in accordance with the experiment. The theoretical ratio of the tensor components is

$$\begin{aligned}\rho_{yy}(y) : \rho^s_{yz}(y) : \rho_{zz}(y) &\fallingdotseq (\sigma_{xx}(y)\sigma_{zz}(y) + \sigma^a_{zx}(y)^2) : \sigma^a_{xy}(y)\sigma^a_{zx}(y) : \\ &(\sigma_{xx}(y)\sigma_{yy}(y) + \sigma^a_{xy}(y)^2) \sim a\sigma^a_{zx}(y)^2 : \sigma^a_{xy}(y)\sigma^a_{zx}(y) : b\sigma^a_{xy}(y)^2 \\ &\sim 1 : 250/a : 60000(b/a), \ (\text{a, } b<10 \text{ and } H\sim 8 \text{ kOe.}).\end{aligned} \tag{24}$$

This is right order of magnitude. $\rho_{zz}(z) - \rho^0_{zz}$, $\rho^s_{yz}(x)$, $\rho^s_{yz}(y)$, and $\rho^a_{xy}(y)$ appear in only the tilted ellipsoid model and the study for these components is useful to elucidate the detail of the energy band structure.

Acknowledgments

The authors express their scincere thanks to Prof. T. Fukuroi, Prof. K. Ariyama and Prof. Y. Shibuya for their kind encouragements and discussions, and also to Mr. K. Tanaka for his kind assistance in the preparation of the samples. One of the authors (S.M.) is also indebted to the Research Institute for Iron, Steel and Other metals which has made him the present study possible. The present study was partly supported by the grant in aid for fundamental scientific research from the Ministry of Education.